

Final Examination

This exam should be answered individually and no contact with other classmates is allowed for the purpose of answering this test. It should be turn in any time before 10:00 am on June13th, and it should be sent via e-mail with the *SUBJECT: Final NMS2020*

1. How do you explain from a thermodynamic point of view the Ostwald ripening phenomenon?

The driving force in the Ostwald ripening process is the decrease of the total surface free energy, where large particles grow at the expense of smaller particles. Ostwald ripening occur by the nucleation and growth of particles from an oversaturated solution. The result are dispersed particles with varying sizes depending on the nucleation rate. The dispersed particles do not meet thermodynamic equilibrium as the particles' configuration is not at the lowest energy due to the excess surface energy. Consequently, the Ostwald ripening process continues to the point where the surface energy is as low as much as possible. The total energy is reduced by the increase of particle size and thus, by the decrease of surface area [1,2].

A solution undergoing the Ostwald ripening process is typically near to the equilibrium of a 2-phase system, but it is not at the lowest energy state possible. The thermodynamic imbalance is due to the polydisperse essence of the mixture and the presence of high surface free energy. The total surface area of the system in time to reach thermodynamic equilibrium. The process by which the particles grow is through diffusion, where mass transfers from particles with high interfacial curvature to particles with low interfacial curvature. Particle growth is triggered by concentration gradients within the solution around the particles. The Gibbs-Thomson relation describes the particle growth by thermodynamic demand, as the concentration at the surface of particles in equilibrium with larger particles is lower than that with smaller particles [1,2].

A system of disperse particles will be thermodynamically unstable due to a large interface area. The system approaches equilibrium by particle coarsening, where the particle solubility depends on the particle radii which described by the Gibbs-Thomson equation [3–5].

$$C_r = C_e \exp \left[\frac{2\gamma\Omega}{RT r} \right]$$

A derivation of the Gibbs-Thomson equation is detailed in Lin et al.'s work [4].

where:

- C_e is the solute concentration at a plane interface in the matrix in equilibrium with particle of infinite radius,
- C_r is the solubility at the surface of a spherical particle with radius r ,
- γ is the specific interfacial energy of the matrix-precipitate particle boundary,
- Ω is the mean atomic (or molar) volume of the particle,
- R is the universal gas constant,
- T is the absolute temperature, and
- r is the particle radius of curvature.

Antonio Osamu Katagiri Tanaka <A01212611@itesm.mx>

2. A nanolayer of atoms are deposited through a chemical reaction on a flat surface and you are asked to develop a general deposition model considering that the reaction can be a first or second order. Assume that both cases are diffusion controlled, the reaction velocity constants (RVCs) are the same and the diffusion rate is X times that of the RVCs. Write the model and make a drawing (by hand) to depict the phenomenon.

[SKIPPED QUESTION]

3. It was found that a soap solution film with an unknown constant thickness reflects the day light and the resulting reflection is blue with a wavelength of 475 nm. The refractive index of the soap solution is 1.4. What is the thickness of the film?

The thickness of soap film solution can be calculated from the thin film interference effect, where light interferes with different surfaces of a thin film. Since interference effects are noticeable when light interacts with structures of similar size to the light wavelength, a thin film shall have a thickness smaller than a few times the wavelength. It is expected to observe different colors at different thicknesses of a film as color is associated with the light wavelength. Thin film interference happens when the light reflected from the top and bottom surfaces of a film interfere with each other as illustrated in Figure 1 [6–8].

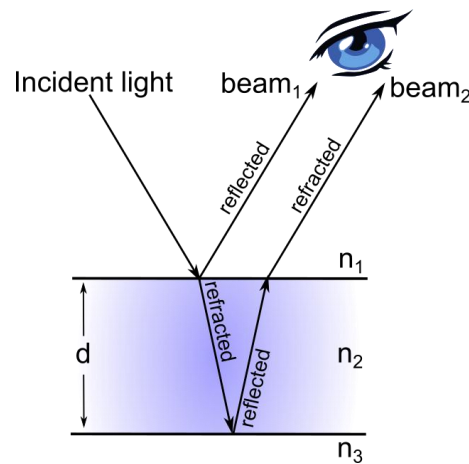


Figure 1 – The incident light is partially reflected at the top surface, and partially refracted to the bottom surface. The refracted beam is partially reflected at the bottom surface and is detected as beam₂. The beam interference depends on the thickness of the film (d) and refraction index of the media (n_1, n_2, n_3). Figure adapted from [6–8].

Then light is reflected from a material with higher refraction index than the material which the light is initially traveling, a $\lambda/2$ shift takes place in the wavelength phase. If the film is a soap bubble, a $\lambda/2$ shift exists for beam₁ and none for beam₂. Beam₂ travels a longer distance than beam₁, around $2d$ farther. When the distance d is a multiple of the wavelength in the medium, thin film interference happens depending on the phase change in either beam [9,10].

Looking back to Figure 1. If the soap thin film has a refraction index of $n_2 = 1.4$ and is surrounded between two media (air), then the light travels some distance inside the film which influences the optical path difference between beam₁ and beam₂. The optical path difference (OPD) is given by $OPD = 2nd$; where n is the refractive index of the soap film and $2d$ is the distance traveled by the light, as d is the thickness of the film. As a wavelength $\lambda/2$ shift takes place, the film adds to the total path difference between the reflected beams of $\Delta = OPD + \frac{\lambda}{2}$. Any constructive beam interference takes place when the path difference is a multiple of the wavelength λ such as $\Delta = m\lambda$. The total path difference is given by [6–8]:

$$2nd + \frac{\lambda}{2} = m\lambda$$

$$2nd = \lambda \left(m - \frac{1}{2} \right); m = 1, 2, 3, \dots$$

The wavelength factor can be amended to $m = 0, 1, 2, \dots$ by substituting $m = m + 1$ as follows:

$$2nd = \lambda \left(m + \frac{1}{2} \right); m = 0, 1, 2, \dots$$

Where,

- d is the thickness of the soap film for the two reflected beams to interfere constructively,
- m is the phase of the interference,
- λ is the light wavelength, and
- n is the refractive index of the soap film.

Substituting the given values in the previous equation, the soap thickness is given by:

$$d = \frac{\lambda}{2n} \left(m + \frac{1}{2} \right); m = 0 \text{ for the minimum thickness}$$

$$d = \frac{475 \text{ nm}}{2(1.4)} \left(\frac{1}{2} \right)$$

$d = 84.821 \text{ nm}$ is the minimum thickness of the film to reflect the blue color.

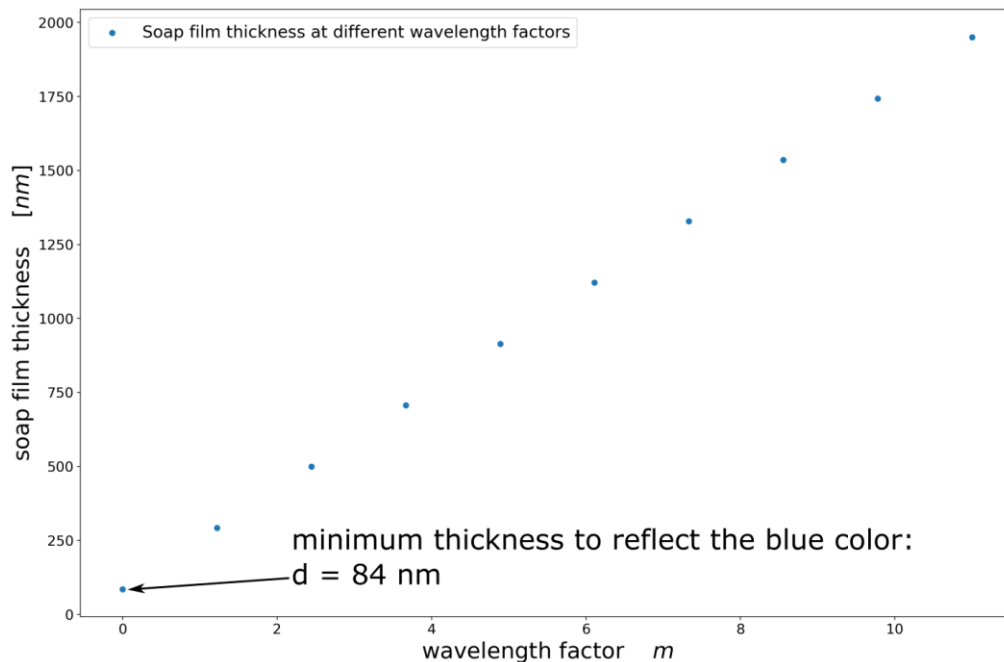


Figure 2 – Various soap film thicknesses that reflect blue light

As shown in Figure 2, the phase of the interference of beam₂ depends on the traveled distance, several film thicknesses can reflect the blue color.

Antonio Osamu Katagiri Tanaka <A01212611@itesm.mx>

4. You obtained a film of gold on a 1 cm² silica wafer. The film is 10 nm thick and you are asked to produce gold nano dots:

The gold nanodot fabrication technique will be based on the thermal dewetting method presented by Li et al. [11]. In their work, they proposed the fabrication of 2D gold nanodot array on a glass substrate. This process is comprised by the following steps:

1. deposition of a metal film on a substrate by sputter coating
2. patterning of a square nano-groove grid on the deposited metal film by the nanoplastic forming (NPF) technique
3. annealing of the patterned substrate in an electric furnace to cause dot aggregation.

The dot size and dot alignment can be controlled by adjusting the nanoplastic forming process parameters, by patterning a grid on the deposited gold film. The NPF is added before annealing into the fabrication process to achieve ordered nanodot arrays of uniform size, as shown in Figure 3.

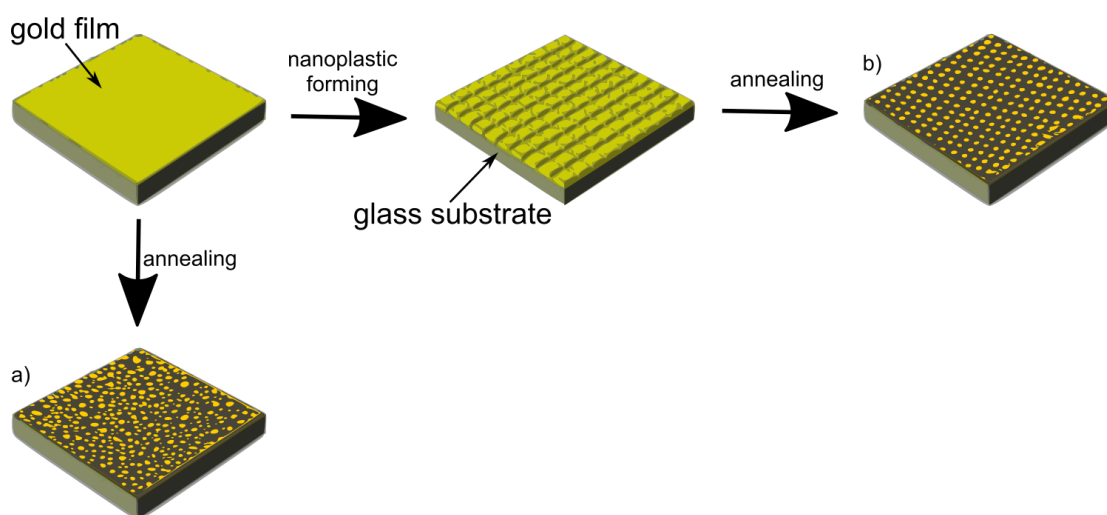


Figure 3 – Nanodot array fabrication process. a) disordered nanodot array annealed without nanoplastic forming. b) ordered nanodot array annealed with nanoplastic forming. Figure adapted from [11]

- a. Write an algorithm of the calculations you must do in order to determine the number of nanodots
 1. First, assume a simplified model of the thermal dewetting process where a plane metal film agglomerates into a single spherical dot.
 2. Then, calculate the nanodot diameter from the diameter of a circular gold film that agglomerates into a single spherical nanodot.
 3. Finally, calculate the number of nanodots given the diameter of a circular gold film that agglomerates into a single spherical nanodot and the total gold film available on the glass substrate (1cm²).

The full calculation is presented in the following paragraphs.

- b. Write the equations, indicating what terms are temperature and surface tension dependent
- c. Show the calculations of how many nanodots you will get.

Note: Do not use the size of nanodots published in the literature to answer this question. However, you can use reported data for surface tension, density, etc.

THEORY:

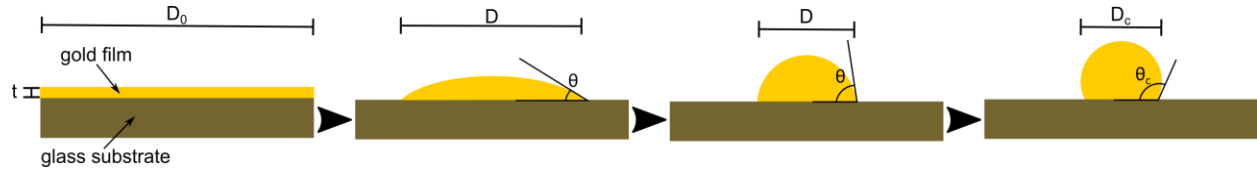


Figure 4 – Thermal dewetting process of a metal film deposited on a substrate. Figure adapted from [12]

As depicted in Figure 4, the thermal dewetting process takes place when a circular metal film of thickness t and diameter D_0 agglomerates into a single spherical particle. D is the transition particle diameter during agglomeration, and D_c is the final dot diameter. The particle's height increases throughout the process as the contact angle θ also increases [13]. The contact angle is related to the surface energy based on Young's equation [14].

$$\gamma_l - \gamma_s = \gamma_M \cos(\theta_c) \quad (1)$$

Where:

- γ_M is the surface energy of gold,
- γ_s is the surface energy of the glass substrate in contact with the dot, and
- γ_l is the surface tension between the gold and the substrate.

Based on Young's equation, the total free energy **before annealing** G_1 of the gold-glass system can be defined as [13]:

$$\begin{aligned} G_1 &= A\gamma_M + A\gamma_l \\ G_1 &= A(\gamma_M + \gamma_l) \end{aligned} \quad (2)$$

Where: $A = \frac{\pi D_0^2}{4}$ (3) is the area of the substrate, such that

$$G_1 = \frac{\pi D_0^2}{4} (\gamma_M + \gamma_l) \quad (4)$$

As the total free energy of the system **during agglomeration** G_2 is comprised by γ_M , γ_s , and γ_l ; it can be calculated as follows [13]:

$$G_2 = S_M\gamma_M + S_l\gamma_l + \gamma_s(A - S_l) \quad (5)$$

Where:

- S_M is the surface area of the gold dot, and
- S_l is the area in contact between the gold and the substrate.

Antonio Osamu Katagiri Tanaka <A01212611@itesm.mx>

When the angle in transition θ is below 90° ,

$$S_M = \frac{\pi D^2}{2} \frac{1 - \cos(\theta)}{\sin^2(\theta)} \quad (6)$$

$$S_l = \frac{\pi D^2}{4} \quad (7)$$

Therefore, substituting (1), (6) and (7) in (5), G_2 is:

$$G_2 = \frac{\pi D^2}{4} \frac{\gamma_M}{1 + \cos(\theta)} [2 - (1 + \cos(\theta)) \cos(\theta_c)] + \frac{\pi D_0^2}{4} \gamma_s \quad (8)$$

The change in surface free energy by agglomeration is given by [13]:

$$\Delta G = G_1 - G_2$$

$$\Delta G = \frac{\pi \gamma_M}{4} \left[D_0^2 (1 - \cos(\theta_c)) - D^2 \frac{2 - \cos(\theta_c) - \cos(\theta) \cos(\theta_c)}{1 + \cos(\theta)} \right] \quad (9)$$

When the angle in transition θ is above 90° [13],

$$S_M = \frac{\pi D^2}{2} (1 - \cos(\theta)) \quad (10)$$

$$S_l = \frac{\pi D^2}{4} \sin^2(\theta) \quad (11)$$

Substituting (1), (10), (11) in (5) gives:

$$G_2 = \frac{\pi D^2}{4} \gamma_M [2 - 2 \cos(\theta) - \sin^2(\theta) \cos(\theta_c)] + \frac{\pi D_0^2}{4} \gamma_s \quad (12)$$

The change/decrease in surface free energy by agglomeration is given by [13]:

$$\Delta G = G_1 - G_2$$

$$\Delta G = \frac{\pi \gamma_M}{4} [D_0^2 (1 - \cos(\theta_c)) - D^2 (2 - \cos(\theta) - \sin^2(\theta) \cos(\theta_c))] \quad (13)$$

On the other hand, the volume of the gold hemisphere can be computed as [13,15,16]:

$$V = \frac{\pi}{24} \frac{D^3}{\sin^3(\theta)} (2 - 3 \cos(\theta) + \cos^3(\theta)) \quad (14)$$

Assuming that the metal volume is conserved throughout the dewetting process as the annealing temperature is above the melting point but below the boiling temperature of the deposited gold, the volume of the hemisphere is equal to the initial gold film volume:

$$V = At$$

$$\frac{\pi}{24} \frac{D^3}{\sin^3(\theta)} (2 - 3 \cos(\theta) + \cos^3(\theta)) = \frac{\pi D_0^2}{4} t \quad (15)$$

Hence, the dot diameter is:

$$D = \sqrt[3]{\frac{6 \sin^3(\theta) D_0^2 t}{2 - 3 \cos(\theta) + \cos^3(\theta)}} \quad (16)$$

CALCULATION:

Assuming the following values:

- $\gamma_M = 1.137 \frac{J}{m^2}$ [17],
- $\gamma_s = 1.37 \frac{J}{m^2}$ [18],
- $t = 10 \text{ nm}$
- $\theta_c = 134^\circ$ at $473K$ [19], and
- $D_0 = 500 \text{ nm}$ [20].

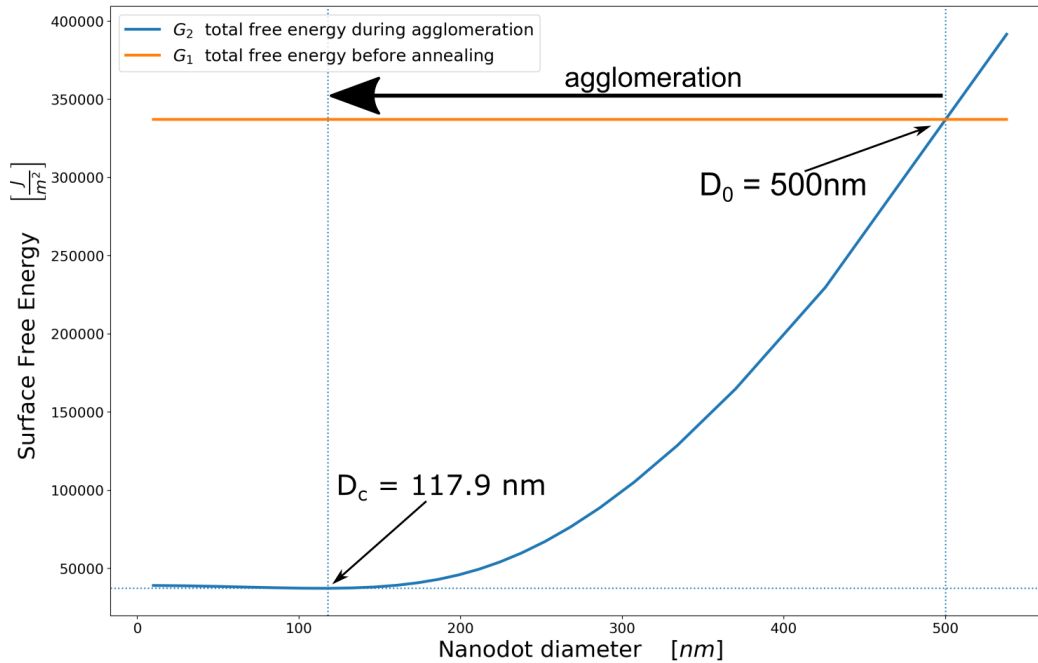


Figure 5 – Surface free energy in function of the gold nanodot diameter

As depicted in Figure 5, the gold nanodot agglomeration starts with a diameter of 500 nm and ends at 117.9005 nm when the surface free energy during agglomeration reaches its minimum value with a contact angle of 134° . Evaluating the assumptions into equation (16) the calculated nanodot diameter is 114.2005 nm . A 3 nm error exists between the analytical and the graphical calculations, which is negligible for the purpose of this examination.

As stated by Yoshino et al. and Iwamatsu [13,15], if the diameter of the substrate D_0 is too small, the gold film is not able to agglomerate into a hemispherical structure. As depicted in Figure 6; if the

initial conditions are the same as in Figure 5 but with a $D_0 = 100 \text{ nm}$, then agglomeration cannot happen as the surface free energy does not decrease below the energy of the system before annealing.

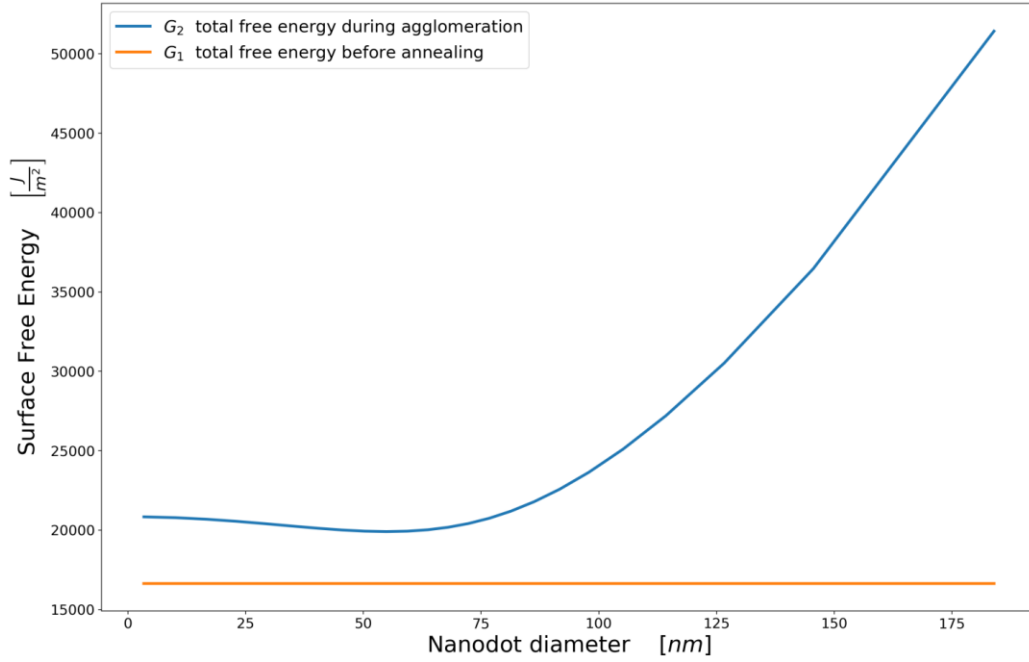


Figure 6 - Surface free energy in function of the gold nanodot diameter. Agglomeration is inhibited as the lowest surface free energy exists before annealing.

Following the simulation of Figure 5, 1 nanodot requires a circular substrate of diameter $D_0 = 500 \text{ nm}$. Therefore, a single gold nanodot needs an area $A = \pi \left(\frac{D_0}{2}\right)^2 \text{ nm}^2 = 62500\pi \text{ nm}^2$. If a film of gold is obtained on a $1 \text{ cm}^2 = 1 \times 10^{14} \text{ nm}^2$ 1 cm² silica wafer, then the number of nanodots is given by:

$$\frac{1 \times 10^{14} \text{ nm}^2}{62500\pi \text{ nm}^2} = 509\,295\,817 \text{ nanodots}$$

A 1 cm² gold film of thickness $t = 10 \text{ nm}$ will yield about 509295817 gold nanodots in a silicon substrate.

d. Determine the % of area the nanodots will have on the 1 cm² silica wafer.

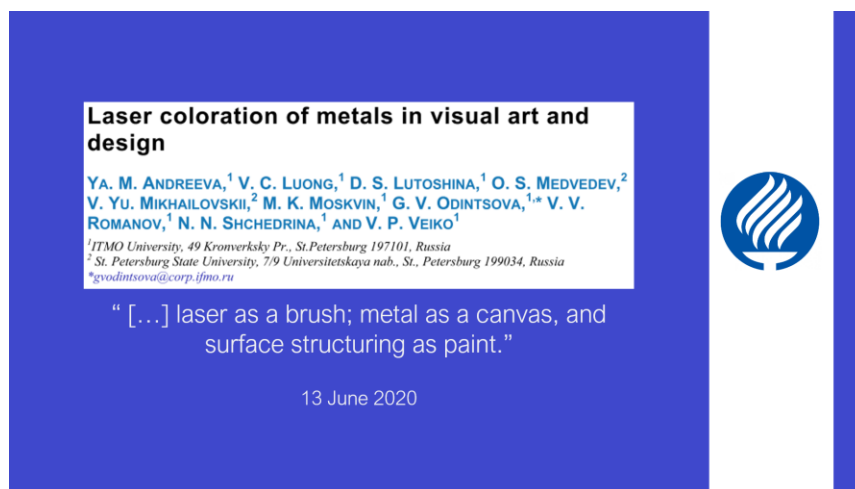
Following the simulation of Figure 5, each gold nanodot will cover an area of $A = \pi \left(\frac{D_c}{2}\right)^2 \text{ nm}^2 = \frac{1390041}{400} \pi \text{ nm}^2$. 509295817 gold nanodots will cover $509295817 \left(\frac{1390041}{400} \pi\right) \text{ nm}^2$. The percentage of area covered by the nanodots in a 1 cm² is given by:

$$100\% \frac{509295817 \left(\frac{1390041}{400} \pi\right) \text{ nm}^2}{1 \times 10^{14} \text{ nm}^2} = 5.56\%$$

The nanodot yield will cover about 5.5% of the area of the silica wafer.

5. You are being interviewed by the CEO of the company Non-Gray Metals, and they asked you make a 3 slide power point presentation based on the paper: "LASER COLORATION OF METALS IN VISUAL ART AND DESIGN" [21]. You should be very careful and need to be very professional on explaining the phenomenon that makes a metal to have different colors.

OPENING SLIDES:



Laser coloration of metals in visual art and design

YA. M. ANDREEVA,¹ V. C. LUONG,¹ D. S. LUTOSHINA,¹ O. S. MEDVEDEV,²
V. YU. MIKHAILOVSKII,² M. K. MOSKVIN,¹ G. V. ODINTSOVA,^{1,*} V. V. ROMANOV,¹ N. N. SHCHEDRINA,¹ AND V. P. VEIKO¹

¹ITMO University, 49 Kronverksky Pr., St.Petersburg 197101, Russia
²St. Petersburg State University, 7/9 Universitetskaya nab., St., Petersburg 199034, Russia
*g.odintsova@corp.ifmo.ru

"[...] laser as a brush; metal as a canvas, and surface structuring as paint."

13 June 2020

As stated by Andreeva et al. several metal coloration techniques have been explored in recent literature, however technologies involving lasers are of more interest due to the wide color palette and the ability to tune the result with high accuracy. The authors present three coloration techniques: a) Metal coloration by laser oxidation of the surface, b) Metal coloration by laser production of silver nanoparticles, and c) Metal coloration by laser structuring of the stainless-steel surface. The three techniques amend the material surface at the nanoscale to control how light is reflected/emitted from the surface. The surface modifications are in accordance with different methods to control the metal coloration.

PRESENTATION BODY:



Metal coloration by laser oxidation

SEM images showing surface structures and their corresponding optical properties:

- 400 nm: $\text{TiO}_2 + \text{Ti}_2\text{O}_3$, $\langle h^* \rangle = 167 \text{ nm}$
- 500 nm: TiO_2 , $\langle h^* \rangle = 61 \text{ nm}$
- 500 nm: TiO_2 , $\langle h^* \rangle = 96 \text{ nm}$
- 500 nm: $\text{TiO}_2 + \text{Ti}_2\text{O}_3$, $\langle h^* \rangle = 223 \text{ nm}$

Schematic diagram illustrating the laser oxidation process on a metal surface, showing incident light, surface structure, and the resulting coloration.

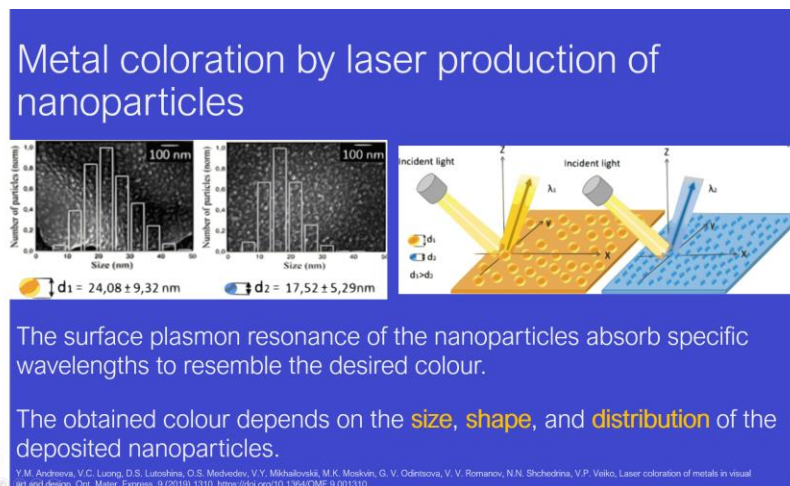
Colour is determined by:

- metal oxide **chemical composition**, and
- oxide **layer thickness**

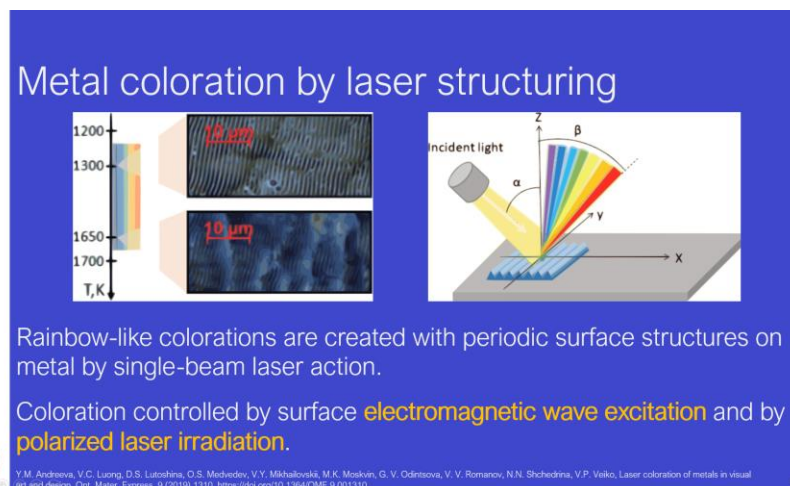
Y.M. Andreeva, V.C. Luong, D.S. Lutoshina, O.S. Medvedev, V.Y. Mikhailovskii, M.K. Moskvina, G. V. Odintsova, V. V. Romanov, N.N. Shchedrina, V.P. Veiko, Laser coloration of metals in visual art and design, Opt. Mater. Express, 9 (2019) 1310. <https://doi.org/10.1364/OME.9.001310>.

Antonio Osamu Katagiri Tanaka <A01212611@itesm.mx>

Metal coloration by laser oxidation of the surface exploits the fact that color is determined by the metal oxide chemical composition (i.e. TiO_2 , Ti_2O_3 , TiO) and the oxide layer thickness. The oxide film thickness is controlled with temperature exposure, which increases with the increasing temperature. Light interactions are depicted in Figure 1.



Metal coloration by laser production of silver nanoparticles by controlling the surface plasmon resonance of deposited nanostructures (metal nanoparticles) on a surface by high-intensive laser irradiation. The desired wavelengths are reflected building-up the wanted color as the surface plasmon resonance of the nanoparticles achieve a selective absorption of the non-desired wavelengths. The obtained color depends on the size, shape, and distribution of the deposited nanoparticles.




Metal coloration by laser structuring of the stainless-steel surface creates rainbow-like coloration with periodic surface structures on metal by single-beam laser action. This technique pretends to achieve the desired coloration by controlling the surface electromagnetic wave excitation and by polarized laser irradiation. Due to the polarized irradiation, the surface coloration depends on the viewing angle

Regardless of the surface modification technique, the smaller the average thickness, particle size or particle distribution; the lower is the wavelength absorbed by the amended surface.


Antonio Osamu Katagiri Tanaka <A01212611@itesm.mx>

CLOSING SLIDES:

“ [...] laser as a brush; metal as a canvas, and surface structuring as paint.”



A graphic featuring the letters 'Q', '&', and 'A' in white, each inside a blue speech bubble. The bubbles are arranged in a row, with the 'Q' bubble on the left, the '&' bubble in the middle, and the 'A' bubble on the right. The background of the graphic is a blurred image of a building.



A small circular logo with a stylized flame or leaf design inside, located in the bottom left corner of the slide.

6

6. Observe the surface of the gold nanoporous film given in the paper “LOCALIZED SURFACE PLASMON RESONANCE OF NANOPOROUS GOLD” [22]. How would you measure the surface tension and the morphology of the film?

The high surface area of nanoporous gold ensembles nanoscale structures and morphologies with special properties. For instance, elastic deformation of nanoporous gold under electrical influence or by unstable gas exposure is achieved by chemical activity [23,24]. Typically, reversible elastic contraction of the nanoporous gold takes place when oxygen is absorbed in thin layers [25]. On the other hand, surfaces of nanoporous gold forms a wetting halo around the interaction of the nanoscale porous material and a liquid drop. The halo size remains constant regardless of the droplet size. Seker et al. [26] described the wetting phenomenon in function of surface tension, shear viscosity and evaporation loss. Following Seker et al.'s [26] work, the nanoporous gold surface tension can be calculated from Young's equation $\Delta\gamma = \gamma_{solid-air} - \gamma_{solid-liquid} = \gamma \cos \theta$. A nanoporous film with a surface area to volume ratio ρ , and thickness h in contact with a liquid droplet will have some free energy per wetted surface area $\Delta\gamma$. Through capillary effect, the droplet moves from the edge of the nanoporous film into it, where x is the traveled distance, see Figure 7.

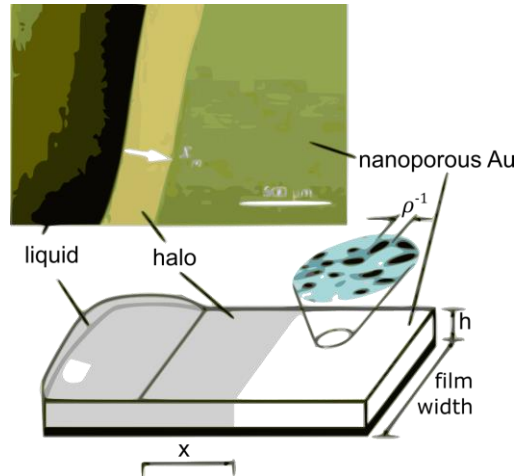


Figure 7 – schematic of the wetting of a droplet on a thin film of nanoporous gold. Figure adapted from [26].

The surface tension per wetted surface area $\Delta\gamma$ can be calculated with [26]:

$$x = \sqrt{\frac{h\beta\Delta\gamma}{8\eta\rho q}}$$

Where:

- β is the void fraction,
- η is the fluid viscosity, and
- q is the difference between the actual and the saturation vapor pressure of the droplet flowing through the nanoporous gold film.

The surface area of nanoporous gold can be measured by electrochemical methods [27], where the impedance and charge density of a porous film is compared to that of a flat film and the

Antonio Osamu Katagiri Tanaka <A01212611@itesm.mx>

difference is used to calculate the surface area. However, some microscopy techniques are more feasible [28–30], as they deliver better analyses of the pore morphology. SEM is the most popular characterization technique, however SEM assumes that a 2D surface can be mapped to extract data of the entire 3D nanoporous gold and the focus shifts on the post-processing of SEM images [31–33]. The first step of a typical image processing algorithm is the selection of a gray-scale image threshold to produce a monochrome image. The issue relays when picking a gray scale value that accurately represents the separation between dark regions of the pores and light regions of the ligaments. The SEM parameters such as working distance, brightness, contrast, and electron acceleration energy should be consistent for each image [34].

7. You want to start your own company on the fabrication of nano-porous membranes. You found the article: “**NANOPOROUS ALUMINUM OXIDE MEMBRANES FOR BIOMEDICAL MICRO HYDRAULIC DEVICES**” [35] to get started but you want to create a **membrane with less pore size dispersion**. What factor would you alter to make the distribution narrower?

High-ordered nanostructures are often characterized by given parameters such as a pore diameter, wall thickness, and barrier layer thickness. The uniform pore diameter is easily controlled by changing the anodizing conditions [36], see Figure 8 [37].

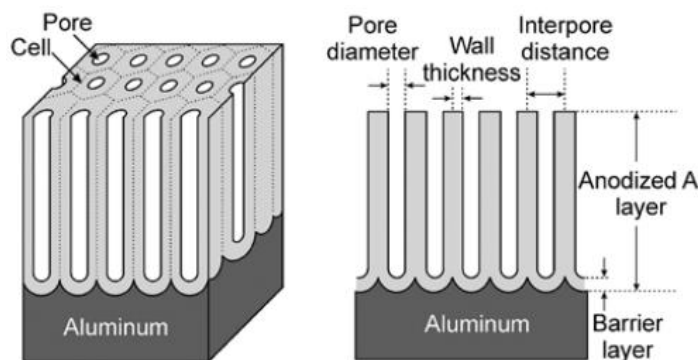


Figure 8 – Structure of anodic porous alumina, indicating the surface parameters of interest to determine uniformity. Figure adapted from [37]

The porous structure develops from the oxide barrier on aluminum at the start of anodization, where the growth of nanopores happens in the presence of high-field ionic conduction at constant field strength [38]. The constant field strength, the uniform aluminum substrate, and the current distribution uniformity are the fabrication parameters that control the pore size uniformity during the growing process. As shown in Figure 9 cracks cause wider size distributions.

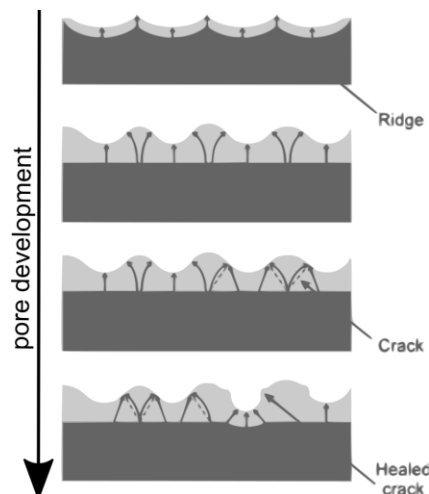


Figure 9 – Development of pores on anodized alumina in the presence of cracks in the Al substrate. Figure adapted from [37].

Narrower pore size distributions are achieved by smoothing the initial roughness of the aluminum by polishing and etching techniques [39–41]. On the other hand, uniformity of oxide growth increases with the increasing purity of aluminum [42]. On the other hand, a three-step anodizing procedure, consisting

Antonio Osamu Katagiri Tanaka <A01212611@itesm.mx>

of two cycles of pre-anodization yield uniform pore diameters with the oxide removal and anodization cycle repetitions. With increasing number of anodization–etching cycles results in an increased uniformity in pore size [43]. Further, the pore diameter increases with increasing anodizing time due to the chemical dissolution of aluminum oxide and to the coalescence and formation of walls [43]. The anodizing duration also alternates the regularity of the self-organized anodic porous alumina structure in such a way that the uniformity of the pore diameter is affected by the chemical attack of the acid.

Therefore, to narrow the pore size distribution three main things are to be done: a) reduce the anodizing time, b) implement a field-assisted technique to achieve uniform current distribution, and c) perform some ‘pure’ aluminum pre-treatment to start with a smooth substrate.

References

- [1] P.W. Voorhees, The theory of Ostwald ripening, *J. Stat. Phys.* 38 (1985) 231–252. <https://doi.org/10.1007/BF01017860>.
- [2] P.W. Voorhees, Coarsening, Modeling Grain Growth, in: *Encycl. Mater. Sci. Technol.*, Elsevier, 2001: pp. 1255–1258. <https://doi.org/10.1016/B0-08-043152-6/00236-9>.
- [3] A. Baldan, Progress in Ostwald ripening theories and their applications in nickel-base super alloys, *J. Mater. Sci.* 37 (2002) 2379–2405. <https://doi.org/10.1023/A:1015408116016>.
- [4] M. Lin, G. Gottstein, L.S. Shvindlerman, Generalized Gibbs-Thomson equation for nanoparticles at grain boundaries, *Acta Mater.* 129 (2017) 361–365. <https://doi.org/10.1016/j.actamat.2017.03.007>.
- [5] J.W. Gibbs, On the equilibrium of heterogeneous substances, *Am. J. Sci.* s3-16 (1878) 441–458. <https://doi.org/10.2475/ajs.s3-16.96.441>.
- [6] C.C. Lee, C.C. Kuo, Optical coatings for displays and lighting, in: *Opt. Thin Film. Coatings From Mater. to Appl.*, Elsevier Ltd, 2013: pp. 564–595. <https://doi.org/10.1533/9780857097316.4.564>.
- [7] R. Grunwald, *Thin Film Micro-Optics*, Elsevier, 2007. <https://doi.org/10.1016/B978-0-444-51746-3.X5000-7>.
- [8] P.P. Urone, R. Hinrichs, K. Dirks, M. Sharma, *College Physics*, OpenStax, 2012. <https://openstax.org/books/college-physics/pages/preface>.
- [9] M. Brindza, R.A. Flynn, J.S. Shirk, G. Beadie, Thin sample refractive index by transmission spectroscopy, *Opt. Express.* 22 (2014) 28537. <https://doi.org/10.1364/OE.22.028537>.
- [10] T.K. Sarma, A. Chattopadhyay, Simultaneous Measurement of Flowing Fluid Layer and Film Thickness of a Soap Bubble Using a UV–Visible Spectrophotometer, *Langmuir.* 17 (2001) 6399–6403. <https://doi.org/10.1021/la010594z>.
- [11] Z. Li, M. Yoshino, A. Yamanaka, Fabrication of three-dimensional ordered nanodot array structures by a thermal dewetting method, *Nanotechnology.* 23 (2012) 485303. <https://doi.org/10.1088/0957-4484/23/48/485303>.
- [12] Q. Xia, S.Y. Chou, The fabrication of periodic metal nanodot arrays through pulsed laser melting induced fragmentation of metal nanogratings, *Nanotechnology.* 20 (2009) 285310. <https://doi.org/10.1088/0957-4484/20/28/285310>.
- [13] M. Yoshino, M. Terano, Fabrication of Metallic Nanodot Arrays, in: 2018: pp. 1–35. https://doi.org/10.1007/978-981-10-6588-0_23-1.
- [14] T. Young, An essay on the cohesion of fluids, *Philos. Trans. R. Soc. London.* 95 (1805) 65–87. <https://doi.org/10.1098/rstl.1805.0005>.
- [15] M. Iwamatsu, Size-dependent contact angle and the wetting and drying transition of a droplet

- adsorbed onto a spherical substrate: Line-tension effect, *Phys. Rev. E*. 94 (2016) 042803. <https://doi.org/10.1103/PhysRevE.94.042803>.
- [16] A. Sommers, A.M. Jacobi, Calculating the Volume of Water Droplets on Aluminum Surfaces, *Int. Refrig. Air Cond. Conf.* (2008) 1–8.
 - [17] S. Dukarov, A. Kryshchal, V. Sukhov, Surface Energy and Wetting in Island Films, *Wetting and Wettability*. (2015). <https://doi.org/10.5772/60900>.
 - [18] N. Martinez, Wettability of silicon, silicon dioxide, and organosilicate glass, 2009. http://digital.library.unt.edu/ark:/67531/metadc12161/m1/1/high_res_d/thesis.pdf.
 - [19] B.P. Azeredo, S.R. Yeratapally, J. Kacher, P.M. Ferreira, M.D. Sangid, An experimental and computational study of size-dependent contact-angle of dewetted metal nanodroplets below its melting temperature, *Appl. Phys. Lett.* 109 (2016) 213101. <https://doi.org/10.1063/1.4968005>.
 - [20] Y. Nakata, K. Murakawa, N. Miyana, A. Narazaki, T. Shoji, Y. Tsuboi, Local Melting of Gold Thin Films by Femtosecond Laser-Interference Processing to Generate Nanoparticles on a Source Target, *Nanomaterials*. 8 (2018) 477. <https://doi.org/10.3390/nano8070477>.
 - [21] Y.M. Andreeva, V.C. Luong, D.S. Lutoshina, O.S. Medvedev, V.Y. Mikhailovskii, M.K. Moskvina, G. V. Odintsova, V. V. Romanov, N.N. Shchedrina, V.P. Veiko, Laser coloration of metals in visual art and design, *Opt. Mater. Express*. 9 (2019) 1310. <https://doi.org/10.1364/OME.9.001310>.
 - [22] X. Lang, L. Qian, P. Guan, J. Zi, M. Chen, Localized surface plasmon resonance of nanoporous gold, *Appl. Phys. Lett.* 98 (2011) 093701. <https://doi.org/10.1063/1.3560482>.
 - [23] D. Kramer, R.N. Viswanath, J. Weissmüller, Surface-Stress Induced Macroscopic Bending of Nanoporous Gold Cantilevers, *Nano Lett.* 4 (2004) 793–796. <https://doi.org/10.1021/nl049927d>.
 - [24] J. Biener, A. Wittstock, L.A. Zepeda-Ruiz, M.M. Biener, V. Zielasek, D. Kramer, R.N. Viswanath, J. Weissmüller, M. Bäumer, A. V. Hamza, Surface-chemistry-driven actuation in nanoporous gold, *Nat. Mater.* 8 (2009) 47–51. <https://doi.org/10.1038/nmat2335>.
 - [25] H.-J. Jin, S. Parida, D. Kramer, J. Weissmüller, Sign-inverted surface stress-charge response in nanoporous gold, *Surf. Sci.* 602 (2008) 3588–3594. <https://doi.org/10.1016/j.susc.2008.09.038>.
 - [26] E. Seker, M.R. Begley, M.L. Reed, M. Utz, Kinetics of capillary wetting in nanoporous films in the presence of surface evaporation, *Appl. Phys. Lett.* 92 (2008) 013128. <https://doi.org/10.1063/1.2831007>.
 - [27] E. Seker, M. Reed, M. Begley, Nanoporous Gold: Fabrication, Characterization, and Applications, *Materials (Basel)*. 2 (2009) 2188–2215. <https://doi.org/10.3390/ma2042188>.
 - [28] R.C. Newman, S.G. Corcoran, J. Erlebacher, M.J. Aziz, K. Sieradzki, Alloy Corrosion, *MRS Bull.* 24 (1999) 24–28. <https://doi.org/10.1557/S0883769400052660>.
 - [29] H. Rösner, S. Parida, D. Kramer, C.A. Volkert, J. Weissmüller, Reconstructing a Nanoporous Metal in Three Dimensions: An Electron Tomography Study of Dealloyed Gold Leaf, *Adv. Eng. Mater.* 9

- (2007) 535–541. <https://doi.org/10.1002/adem.200700063>.
- [30] T. Fujita, L.-H. Qian, K. Inoke, J. Erlebacher, M.-W. Chen, Three-dimensional morphology of nanoporous gold, *Appl. Phys. Lett.* 92 (2008) 251902. <https://doi.org/10.1063/1.2948902>.
 - [31] E. SEKER, M. REED, M. BEGLEY, A thermal treatment approach to reduce microscale void formation in blanket nanoporous gold films, *Scr. Mater.* 60 (2009) 435–438. <https://doi.org/10.1016/j.scriptamat.2008.11.027>.
 - [32] R. Li, K. Sieradzki, Ductile-brittle transition in random porous Au, *Phys. Rev. Lett.* 68 (1992) 1168–1171. <https://doi.org/10.1103/PhysRevLett.68.1168>.
 - [33] Z. Li, S. Zhuo, H. Li, W. Si, Y. Ding, Determination of Ligament Size Distribution of Nanoporous Gold by Scanning Electron Microscopy and Image Analysis, *J. Nanosci. Nanotechnol.* 9 (2009) 1651–1654. <https://doi.org/10.1166/jnn.2009.C224>.
 - [34] F. Dias, Thresholding Using the ISODATA Clustering Algorithm, *IEEE Trans. Syst. Man. Cybern.* 10 (1980) 771–774. <https://doi.org/10.1109/TSMC.1980.4308400>.
 - [35] G. Janusas, A. Guobiene, A. Palevicius, L. Ramalis, Nanoporous aluminum oxide membranes for biomedical micro hydraulic devices, *Vibroengineering PROCEDIA*. 15 (2017) 110–114. <https://doi.org/10.21595/vp.2017.19448>.
 - [36] H. Masuda, H. Yamada, M. Satoh, H. Asoh, M. Nakao, T. Tamamura, Highly ordered nanochannel-array architecture in anodic alumina, *Appl. Phys. Lett.* 71 (1997) 2770–2772. <https://doi.org/10.1063/1.120128>.
 - [37] G.D. Sulka, Highly Ordered Anodic Porous Alumina Formation by Self-Organized Anodizing, 2008. <https://doi.org/10.1002/9783527621507.ch1>.
 - [38] G.. Thompson, Porous anodic alumina: fabrication, characterization and applications, *Thin Solid Films*. 297 (1997) 192–201. [https://doi.org/10.1016/S0040-6090\(96\)09440-0](https://doi.org/10.1016/S0040-6090(96)09440-0).
 - [39] M.K. Kushwaha, A comparative Study of Different Electrolytes for Obtaining Thick and Well-ordered nano-porous Anodic Aluminium Oxide (AAO) Films., *Procedia Mater. Sci.* 5 (2014) 1266–1273. <https://doi.org/10.1016/j.mspro.2014.07.438>.
 - [40] O’SULLIVAN JP, WOOD GC, The morphology and mechanism of formation of porous anodic films on aluminium, *Proc. R. Soc. London. A. Math. Phys. Sci.* 317 (1970) 511–543. <https://doi.org/10.1098/rspa.1970.0129>.
 - [41] G.E. THOMPSON, R.C. FURNEAUX, G.C. WOOD, J.A. RICHARDSON, J.S. GOODE, Nucleation and growth of porous anodic films on aluminium, *Nature*. 272 (1978) 433–435. <https://doi.org/10.1038/272433a0>.
 - [42] L.. Fratila-Apachitei, H. Terryn, P. Skeldon, G.. Thompson, J. Duszczyk, L. Katgerman, Influence of substrate microstructure on the growth of anodic oxide layers, *Electrochim. Acta*. 49 (2004) 1127–1140. <https://doi.org/10.1016/j.electacta.2003.10.024>.

Antonio Osamu Katagiri Tanaka <A01212611@itesm.mx>

- [43] C. Brändli, T.F. Jaramillo, A. Ivanovskaya, E.W. McFarland, Automated synthesis and characterization of diverse libraries of macroporous alumina, *Electrochim. Acta.* 47 (2001) 553–557. [https://doi.org/10.1016/S0013-4686\(01\)00778-2](https://doi.org/10.1016/S0013-4686(01)00778-2).